Metal Vaporization from Weld Pools

A. BLOCK-BOLTEN and T. W. EAGAR

Experimental studies of alloy vaporization from aluminum and stainless steel weld pools have been made in order to test a vaporization model based on thermodynamic data and the kinetic theory of gases. It is shown that the model can correctly predict the dominant metal vapors that form but that the absolute rate of vaporization is not known due to insufficient knowledge of the surface temperature distribution and subsequent condensation of the vapor in the cooler regions of the metal. Values of the net evaporation rates for different alloys have been measured and are found to vary by two orders of magnitude. Estimated maximum weld pool temperatures based upon the model are in good agreement with previous experimental measurements of electron beam welds.

I. INTRODUCTION

LOSS of alloying elements from the weld pool due to vaporization is important for a number of reasons. Firstly, if the loss is great enough, the mechanical properties of the weld may be impaired.[1] Secondly, the composition of a welding arc plasma influences the temperature of the arc,[2] arc stability, and fume formation.[3] Thirdly, it has been shown that vaporization places an upper limit on the temperature produced on the surface of the metal due to evaporative cooling.[4,5]

A previous paper has presented a formalism for calculation of partial pressures of metal vapors above steel weld pools.[5] This analysis provided an estimate of the power lost by evaporation as well as an upper bound on the surface temperature of steel weld pools as a function of alloy composition. In the present paper, this analysis is extended to evaporation from aluminum and copper alloy weld pools where different metal vapors dominate. The results of the calculations are then compared with experimental results from both aluminum and steel weld metals.

II. EXPERIMENTAL PROCEDURE

Both steel samples and aluminum alloy samples were subjected to extended time welding in a specially adapted chamber which was coupled to a direct reading emission spectrometer. The chamber was supplied with a lens guiding the light to the spectrometer grating. A mirror imaging device was provided to ensure uniform position of the work and the electrode. The hearth was water cooled and the entire system was purged with argon flow. The rotating water-cooled copper hearth shown in Figure 1 was employed in the case of 12.5 cm diameter 304 steel samples, but the rotation has not proven useful. The slight deviations of the rotating sample cause periodic sinusoidal changes in the arc length and corresponding oscillations in the spectral signal. Therefore, this experiment could be characterized only by lower and upper limits of spectrographic signal, voltage, current, and final weld chemical composition, and not by a uniquely defined value of each of those parameters. As a result, the experimental data presented in this paper were obtained from stationary arc welds where the arc length was more controllable.

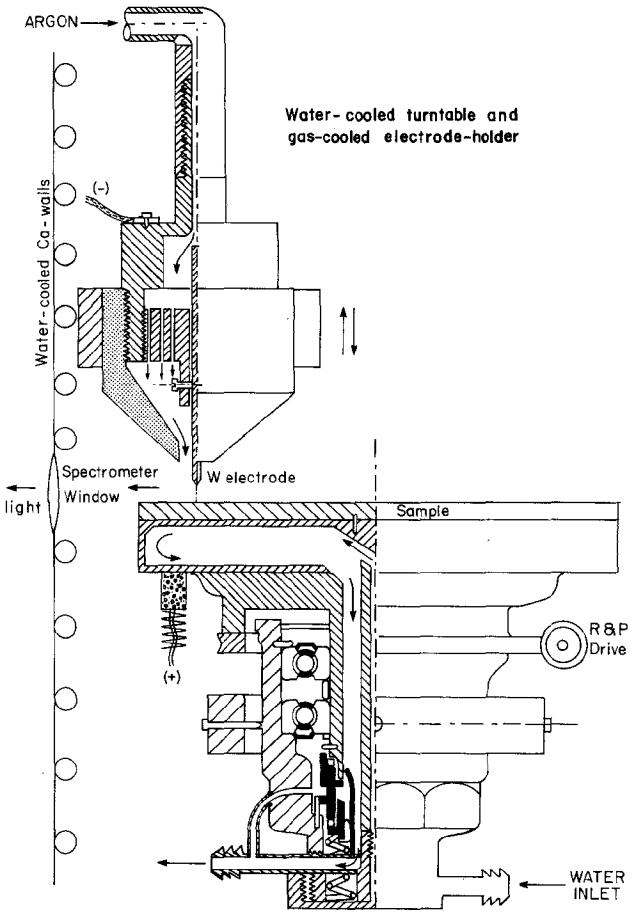

Fig. 1 — Water-cooled turntable and gas-cooled electrode holder.

The 0.35 to 1.10 g steel samples consisted of 1.6 mm diameter wires (502, 505, 5151, and 5212 steels) or 1.1 mm wire (410 steel) or 2.4 mm diameter wires (308L and 309L steels). The thoriated tungsten electrodes of 1.6 mm diameter were mounted as shown in Figure 1. Each steel sample was weighed before and after each experiment, yet only the 308L and 309L stainless steel samples gave reasonable weight loss results (Figure 2), as other steels were too readily oxidized in spite of the welding grade argon environment. The small amount of impurities in this gas stream and the extended time of these tests created a significant weight

A. BLOCK-BOLTEN, Research Scientist, is now with the Department of Metallurgy and Materials Science, University of Toronto. T. W. EAGAR, Associate Professor, Materials Engineering, is with the Department of Materials Science and Engineering, Massachusetts Institute of Technology, Cambridge, MA 02139.

Manuscript submitted September 23, 1983.

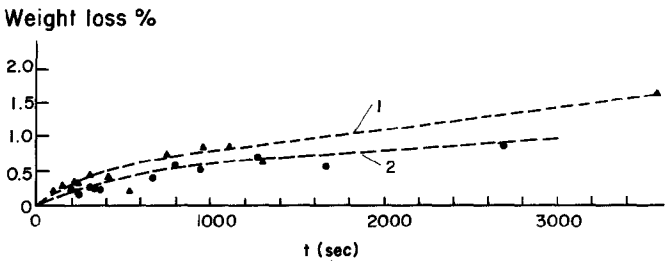

Fig. 2—Weight-loss experiment. 1—weight loss curve for 308L stainless steel, 2—for 309L stainless steel; average voltage 11 V, current set at 15 A; average sample size 1 g.

loss or gain by oxidation over the course of the experiment in these other steels. The compositions of the steel and Al-alloy samples used are given in Table I. The sizes of the Al-alloy samples are specified in the caption of Figure 8.

Atomic absorption chemical analysis was performed on buttons from the melted steel wires and on shavings drilled out of craters of the Al-alloy samples after melting.

The spectrographic signals were ratioed relative to the most abundant element of the alloy: Fe in steels and Al in Al-alloys, through a system of analog dividers. The spectrographic signals from the photomultipliers were measured by Keithley Model 480 picoamperometers.

III. PREDICTION OF VAPORIZATION TENDENCY

As shown in a previous paper,[5] the logarithm of the partial pressure of an alloy component in the gas phase is proportional to the sum of the logarithms of the standard pressure of the pure element and the activity of the element in the alloy, *i.e.*,

$$\log \bar{p}_A = \log p_A^\circ + \log a_A \qquad [1]$$

where

$\bar{p}_A$ is the partial pressure of element A in the gas phase,
p_A° is the standard pressure of pure A, and
a_A is the activity of A in the alloy.

The vaporization rate can be predicted from the kinetic theory of gases,[6]

$$r_A = 44.331 \bar{p}_A \left(\frac{M_A}{T}\right)^{1/2} [\text{g} \cdot \text{s}^{-1} \cdot \text{cm}^{-2}] \qquad [2]$$

where

r_A is the rate of evaporation of element A,
M_A is the molecular weight of A,
T is the absolute temperature, and
$\bar{P}_A$ has units of atmospheres.

The evaporation power loss P_L is then

$$P_L = r_A(L_A - \overline{\Delta H}_A)[\text{watt} \cdot \text{cm}^{-2}] \qquad [3]$$

where

L_A is the heat of evaporation of pure A and
$\overline{\Delta H}_A$ is the partial molar heat of mixing of A in the alloy.

The evaporative energy loss, E_L, is

$$E_L = r_A(L_A - \overline{\Delta H}_A)t[\text{watt cm}^{-2}\text{ s}], \qquad [4]$$

where t is time. In most cases $\overline{\Delta H}_A$ is small compared to the heat of evaporation. If the element of interest is the solvent such as iron in steel or aluminum in aluminum alloys, $\overline{\Delta H}_A$ can be neglected.

Using Eq. [1], it is possible to construct pressure-temperature diagrams for aluminum, copper, and iron base alloys as shown in Figures 3, 4, and 5. These diagrams

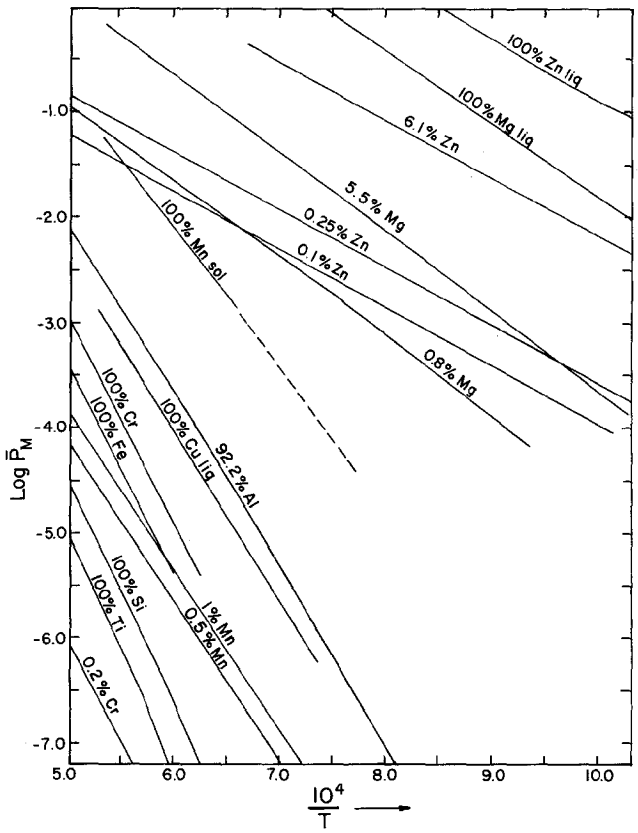

Fig. 3—Aluminum alloys: vapor pressures for some constituent alloy additions.

Table I. Compositions of Starting Materials Used in This Study

Steels: Compositions As Delivered				Al Alloys: Composition As Delivered		
Steel Number	Pct Fe	Pct Mn	Pct Cr	Alloy Number	Pct Zn	Pct Mg
410	86.70	0.45	12.03	7075	5.82	2.30
502	94.87	0.45	4.00	5083	0.014	4.06
505	89.70	0.45	9.06	5456	0.019	5.20
5151	98.05	0.54	0.99/1.37	6061	0.063	0.95
5212	97.30	0.55	1.91	2024	0.058	1.46
308L	67.25	1.91	21.00	1100	<0.010	<0.010
309L	59.65	1.79	26.08			
304	68.80	1.75	18.66			

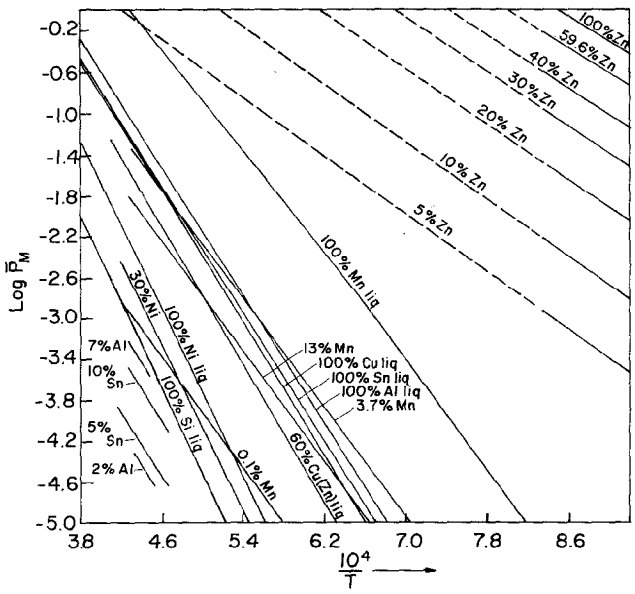

Fig. 4—Copper alloys: vapor pressures for some constituent alloy additions.

are based on tabulated values of activity coefficients.[12] To extrapolate Hultgren's activity (a_0) data to other (a_n) temperatures, $\log a_n = \log a_0 + \overline{\Delta G}^{xs}(To - Tn)/4.575\,ToTn$, $\overline{\Delta G}^{xs}$ was assumed identical to $\overline{\Delta H}$, and $\overline{\Delta G}^{xs}$ or $\overline{\Delta H}$ was used, whichever was available. $\overline{\Delta G}^{xs}$ is partial excess free energy of mixing.

As shown previously, mild interaction effects between the alloying elements in ternary and higher order systems can often be neglected;[5] however, strong interactions where compounds tend to form in the liquid metal cannot be neglected.

As shown previously for steels,[5] Eq. [4] can be combined with the arc surface energy distributions of Nestor[7] to produce upper limits on the surface temperature of the weld pool. Figure 6 shows such an upper bound analysis for a number of aluminum alloys. The upper bound analysis assumes that all of the power input to the weld pool is lost by vaporization of the metal. Since this is clearly not true, a least upper bound on the temperature of the weld pool surface can be obtained if one knows what fraction of the total input power is lost by evaporation. As will be shown later, it is difficult to measure this quantity with precision. The concept of the upper bound temperature of the pool is outlined in a previous paper.[5]

IV. CORRELATION OF THEORY WITH EXPERIMENT

As noted in the experimental procedure section, a number of steel and aluminum alloys were arc melted for unusually long times in order to evaporate enough alloying components to be detectable by chemical analysis. Due to problems of oxidation, only two of the stainless steel samples gave consistent results. The Mn and Fe spectrographic signals normalized to the relatively stable Cr signals as a

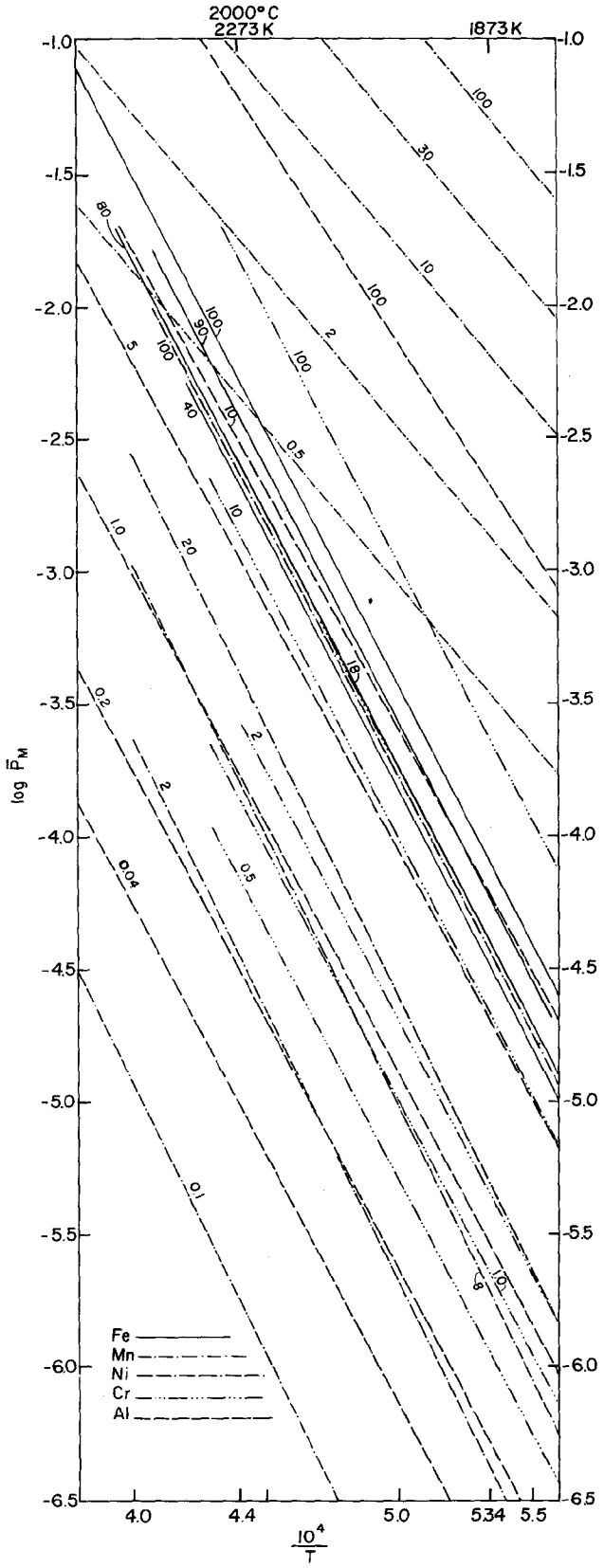

Fig. 5—Steels: vapor pressures for some constituent alloy additions. Numbers on curves represent weight percentages.

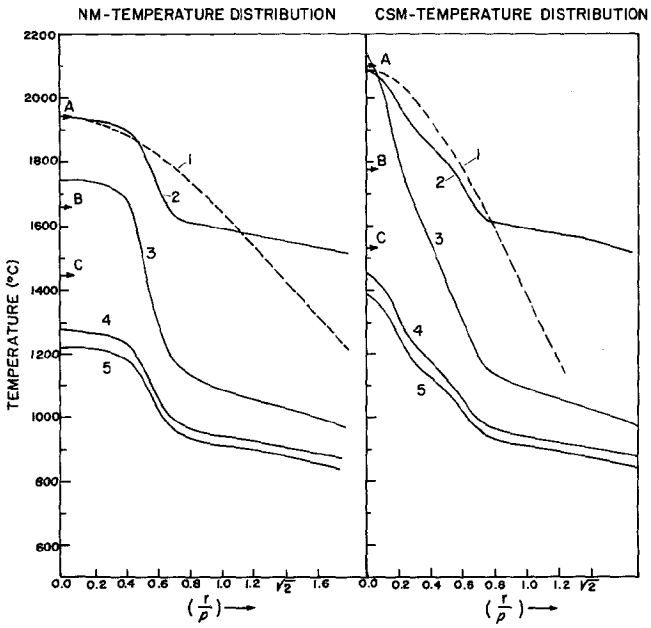

Fig. 6—Normal mode and cathode spot mode temperature distributions for the 5456 Al-alloy. The temperature is plotted *vs* non-dimensional distance r/ρ from the center of the arc; ρ is defined as in Ref. 5 as $\rho = \sqrt{V/2\pi C}$ where V is the total power of the arc (in watts) and C is the peak power density in watt · cm^{-2}. The plots are based on Fig. 3 and on Nestor's[7] power distribution curves. Should 100 pct of energy go into evaporation of pure aluminum, point A on temperature ordinate would correspond to the expected maximum temperature of the weld pool. Points B and C mark 10 pct and 1 pct energy going into evaporation, respectively. Curves 1 are normal distribution (of energy) curves for pure aluminum. Curves 2 are those based on Nestor for pure Al. Curves 3 are for evaporation of 0.25 pct Zn in Al, and curves 4 and 5 are for evaporation of 4.7 pct Mg in Al and 5.5 pct Mg in Al, respectively.

function of arc melting time are shown in Figure 7. It will be noted that Mn is the primary element lost as predicted by Figure 5.

In order to test the model more completely, a series of six aluminum alloys with varying zinc and magnesium contents were selected. Aluminum alloys were selected because the Zn and Mg have very high vapor pressures as compared to aluminum; and as seen in Figure 6, this significantly lowers the upper bound temperature.

The aluminum alloys can be separated into four groups, where

I Zn vapor dominates,
II Mg vapor dominates,
III nearly equivalent Zn and Mg vapor pressure exists,
IV Al vapor dominates.

Alloy 7075 belongs in group I as seen in Figure 8. If we compare Table II and Figure 3, we see that the high zinc concentration in 7075 alloy places the zinc isopleth of Figure 2 well above the Mg isopleth for this alloy.

Alloys 5083 and 5456 belong to group II as seen in Figures 9 and 10. This is again consistent with the predictions made from Table II and Figure 3.

Alloys 6061 and 2024 belong to group III as shown in Figures 11 and 12, respectively. This result is not as easily predicted from Figure 3 since the exact composition of the alloy and the temperature of the weld pool surface are not known precisely. Nonetheless, the spectrographic data of Figure 13 clearly show a simultaneous rise in the spectral signals for both Mg and Zn. It is interesting to note that Zn typically reaches its maximum presence in the vapor later than Mg, probably due to kinetic limitations since Zn is more dilute in the alloy. The gradual rise of both elements

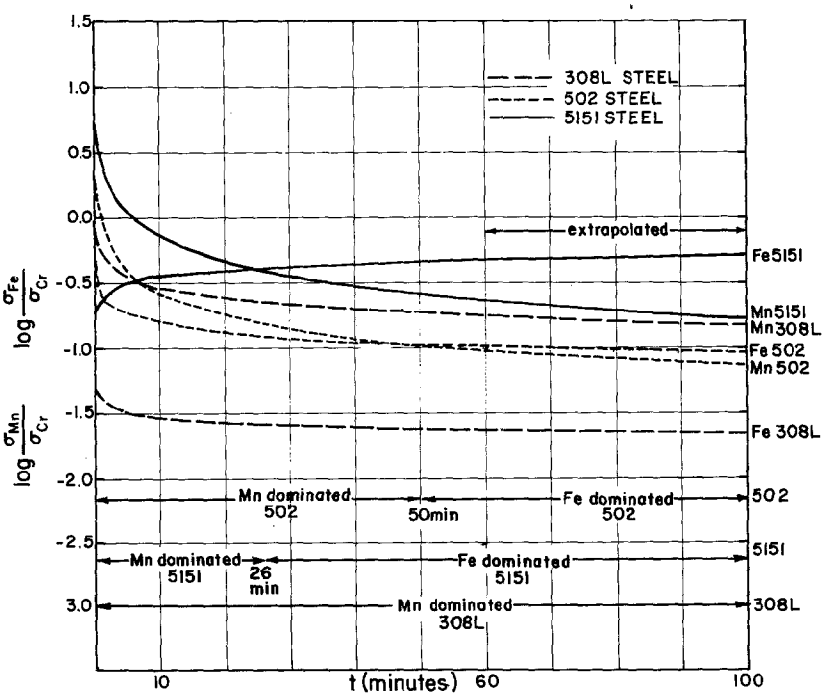

Fig. 7—Decay of normalized signal ratios of iron to chromium and manganese to chromium (Cr content does not change significantly) for three different steels. As can be seen, Mn dominates over the iron in the vapor phase. Only after long periods of time does iron start to dominate in the 5151 and 502 steels.

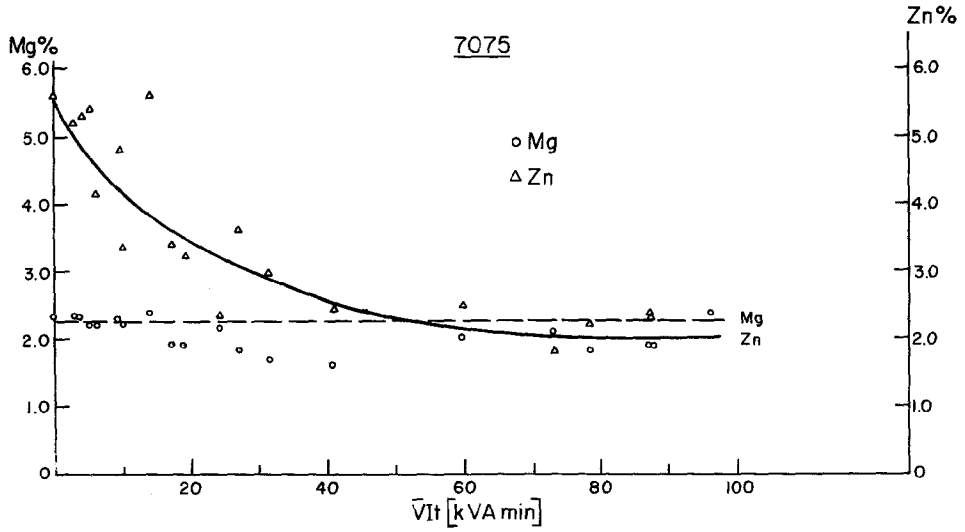

Fig. 8—Loss of Zn *vs* energy input in [KVA min] from aluminum alloy 7075. No change in Mg was found. Original contents of Mg and Zn were 2.3 pct and 5.6 pct, respectively. The voltage during tests varied between 12.5 and 15 V; current was set between 125 A and 150 A; the longest experiment lasted 45 min. The size of the samples was 52 × 51 × 12.7 mm. Rates of evaporation for this and other alloys are given in Table III.

Table II. Calculated Center Line Surface Temperature of Weld Pools for Six Aluminum Alloys

1100 Alloy, 0 to 0.1* Pct Zn, Bal. Al			2024 Alloy, 0.25 Pct Zn; 1.2 to 1.8* Pct Mg			5083 Alloy, 0.25 Pct Zn; 4 to 4.9* Pct Mg		
Power Density, Pct	Vapor Domination	*t* °C Range NM/CSM	Power Density, Pct	Vapor Domination	*t* °C Range NM/CSM	Power Density, Pct	Vapor Domination	*t* °C Range NM/CSM
100	Al	1935*/2091	100	Mg	1422*/1751	100	Mg	1268*/1491
10	Zn*, Al	1364*/1614	10	Mg	1101*/1290	10	Mg	994*/1126
1	Zn*, Al	968*/1530	1	Zn, Mg*[CSM]	870*/ 975	1	Mg	807*/ 905
5456 Alloy, 0.25 Pct Zn; 4.7 to 5.5* Pct Mg			6061 Alloy, 0.25 Pct Zn; 0.8 to 1.2* Pct Mg			7075 Alloy, 5.1 to 6.1* Pct Zn; 2.1 to 2.9 Pct Mg		
Power Density, Pct	Vapor Domination	*t* °C Range NM/CSM	Power Density, Pct	Vapor Domination	*t* °C Range NM/CSM	Power Density, Pct	Vapor Domination	*t* °C Range NM/CSM
100	Mg	1220*/1451	100	Mg	1513*/1882	100	Zn	1057*/1242
10	Mg	964*/1104	10	Zn, Mg*	1154*/1358	10	Zn	795*/ 909
1	Mg	783*/ 891	1	Zn	870*/ 994	1	Zn	612*/ 695

Normal Mode NM 200 A, 14.0 V, $C = 2180$ [watt · cm^{-2}]
Cathode Spot Mode CSM 200 A, 14.8 V, $C = 6120$ [watt · cm^{-2}] peak power density
*Note that the lower calculated temperatures correspond to the higher alloy compositions.

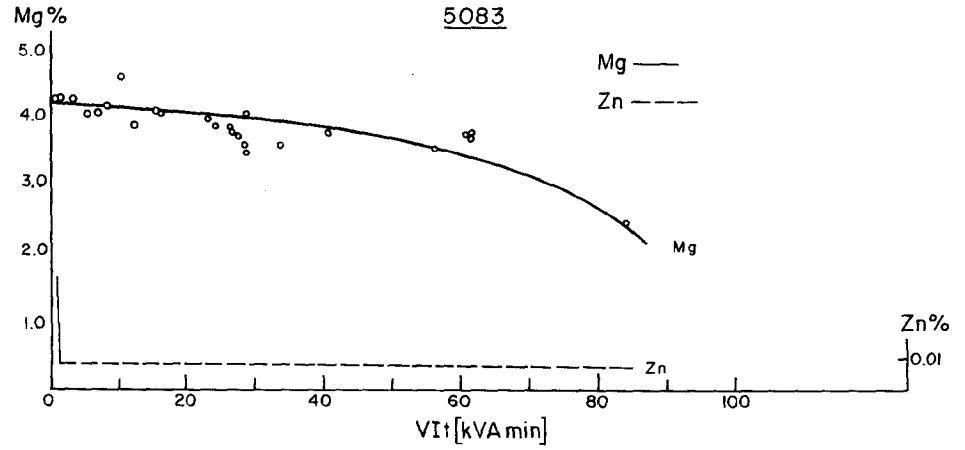

Fig. 9—Aluminum alloy 5083. Loss of Mg *vs* energy input. The change in Zn content occurs only in the first few seconds of the experiment, then Zn remains constant. The original Mg content was 4.3 pct. Voltage and current were 15 V and 125 A. The longest experiment lasted 45 min.

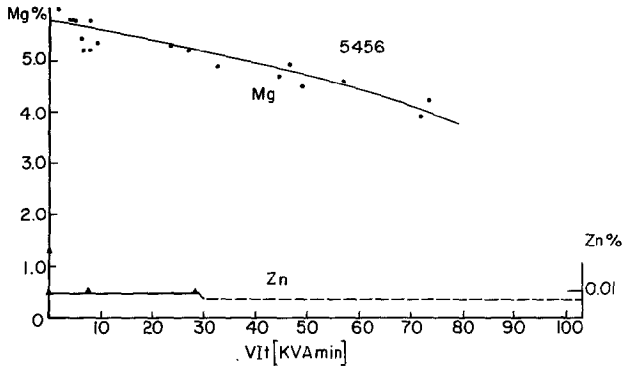

Fig. 10—Aluminum alloy 5456. Loss of Mg *vs* energy input. The changes in Zn content occur only in the first seconds of the experiment, then Zn remains constant. Original Mg content 5.8 pct. Average voltage was 15 V, and current was set between 125 and 150 A. The longest experiment lasted 45 min.

is most likely due to increase in the size of the weld pool with time. Alloy 1100 is the only sample tested which belongs to group IV of the series.

Summarizing, Figures 8 to 12 show the analyses taken from the weld pools of different Al-alloys during extended time welding. The 7075 alloy with Zn-vapor domination (Figure 8) exhibits changes only in Zn content, while Mg content stays constant. In Figures 9 and 10, the Mg-vapor dominated 5083 and 5456 alloys show Mg-content falling off, while Zn-content stays constant or below the detection level. Figures 11 and 12 for alloys 6061 and 2024 prove that both these alloys exhibit mixed vapor domination and both Zn and Mg contents change with time. In addition, SEM semiquantitative analyses have also shown changes in Zn only for the 7075 alloy, changes in Mg only for 5083 and 5456 alloy, and changes both in Mg and Zn content for the 2024 and 6061 alloys.

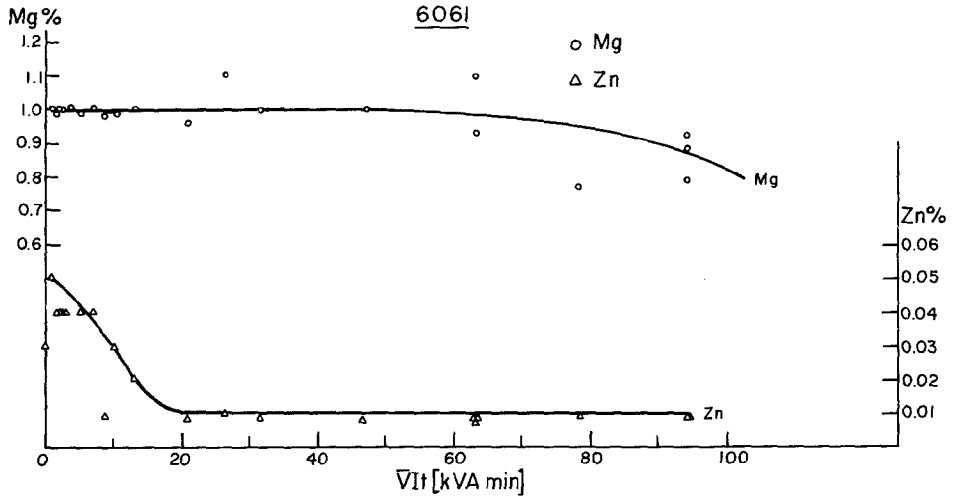

Fig. 11—Aluminum alloy 6061. Loss of Mg and Zn *vs* energy input. Original Mg content was 0.95 pct and the original Zn content 0.06 pct. Average voltage 14 V; the current was set at 150 A. Longest experiment lasted 45 min.

Table III. Net Energy Lost from Weld Pool by Evaporation of Alloying Elements

Group	Al-Alloy	Evaporating Element	Apparent Initial Net Evaporation Rate [$\mu g s^{-1} cm^{-2}$]	Apparent Long-Term (Mean) Evaporation Rate [$\mu g s^{-1} cm^{-2}$]	Theoretical Evaporation Energy $(L-\Delta H)^{-1}$ [$\mu g J^{-1}$]	Apparent Evaporation per Gross Energy Input* [$\mu g J^{-1} \times 10^3$]	Percent of Arc Energy Lost by Evaporation	Source of Data (Figure No.)
I	7075	Zn	94.9	30.5	631.1	91.4	0.0144	8
		Mg	—	—	173.5	—	—	
II	5083	Zn	(11.3)	~0	631.1	38.0	0.0060	9
		Mg	5.6	12.1	173.5	40.6	0.0235	
	5456	Zn	—	~0	631.1	—	—	10
		Mg	9.7	12.7	173.5	49.0	0.0280	
		Al**	0	(90 to 230)	92.8	—	—	
III	6061	Zn	1.2	1.2	631.1	3.6	0.0006	11
		Mg	0	1.2	173.5	3.6	0.0021	
	2024	Zn	12.0	1.3	631.1	3.8	0.0006	12
		Mg	10.0	3.4	173.5	3.4	0.0020	

*gross energy input, Refs. 8, 9
**from soot formation and Al-ball growth

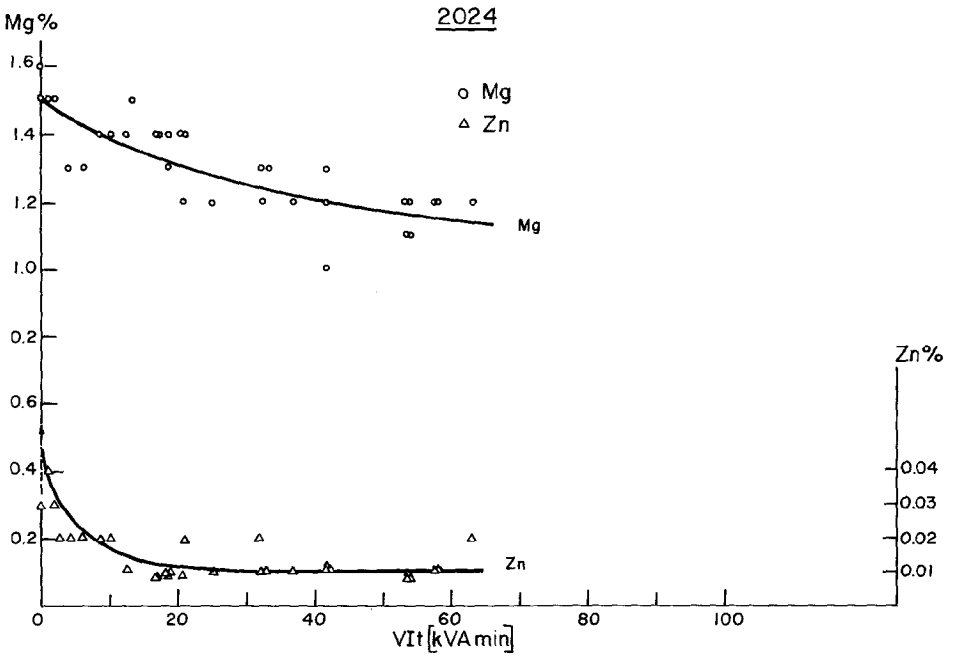

Fig. 12—Aluminum alloy 2024. Loss of Mg and Zn content *vs* energy input. Original Mg content 1.5 pct, Zn content 0.06 pct. Average voltage was 14 V, and the current was set at 150 A. Longest experiment lasted 30.2 min.

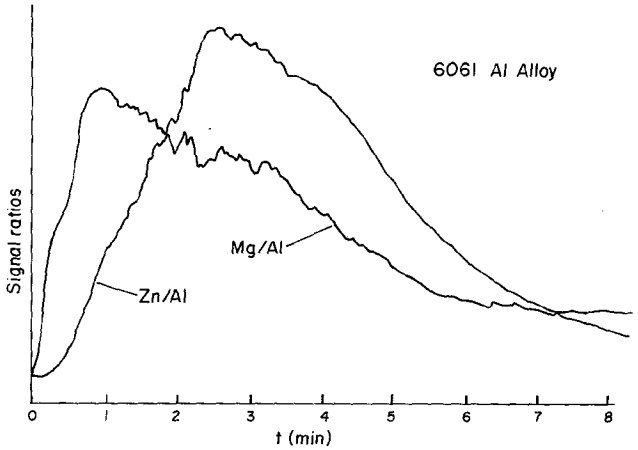

Fig. 13—Signal ratios of Mg and Zn normalized to aluminum, as typically observed for the 6061 aluminum alloy. The Mg/Al signal ratio is magnified 10 times.

From Figures 8, 9, 10, 11, and 12, values of apparent initial evaporation rate, apparent long term (mean) evaporation rate, and apparent evaporation per unit of energy have been calculated. The latter value is normalized to gross energy input[8,9] which is half of the total arc power input, as the other half is lost to the environment and does not enter the weld pool. All these values, together with percentages (referred to theoretical evaporation per unit energy $(L - \overline{\Delta H})^{-1}[J^{-1}]$) are displayed in Table III. It is seen that the net power lost by vaporization is much less than one percent of the total power input to the metal. As will be discussed later, this is much less than the absolute evaporative power loss; however, much of the absolute evaporative power is regained by condensation of the vapors in cooler regions of the weld pool.

V. DISCUSSION

The preceding results indicate that the model can effectively use existing thermodynamic data to predict the dominant metal vapors above the weld pool; however, it would be useful if one could predict weld pool surface temperature and hence the rate of alloy element loss. This proves to be a much more difficult task.

Quigley, *et al.*[9] have estimated the evaporative power loss from a gas tungsten arc to be of the order of 2 pct of the total power. If this is true, it would reduce the upper bound temperatures based on 100 pct evaporative power loss as shown in Figure 6 and in Table II. Indeed, if one were to assume absolute evaporative power loss to lie between 1 and 10 pct of the total power, the surface temperature limit would drop by 200 to 500 °C for aluminum alloys. Table II shows that the surface temperature of aluminum alloy arc welds could vary from just above the melting temperature to 700 °C superheat depending on alloy composition and the amount of heat lost by vaporization.

As shown in Table III and Figures 8 though 12, weight loss measurements based on alloying element loss from the weld samples gives net evaporative losses between zero and $95[\mu g \cdot s^{-1} \cdot cm^{-2}]$. This corresponds to maximum net vaporization losses of roughly 0.015 pct of the net incident power; however, it is believed that more metal than this is vaporized from the center of the pool and then recondenses on cooler regions, thus recycling through the system. This is indirectly confirmed by spectrographic monitoring of calcium vapor in 304 stainless steels.[10] The calcium spectrographic lines remain strong and do not diminish after 15 minutes of welding even though there is only 10 ppm Ca in the steel. The only way this small amount of Ca could remain after such a long time is if it is "recycled" into the metal by condensation. Although it is not possible to measure how much vapor condenses back into the pool rather

than is lost, it is believed that a larger fraction of Zn recondenses back to the pool than is lost from the system. In a sense, this is confirmed by the temperatures calculated for the 7075 alloy in Table II. If the temperature were low enough for only 0.015 pct of the power to be lost by vaporization, then the liquid would be cool enough to solidify. It is clear that at least several percent of the power at the center of the 7075 alloy pool must be lost by zinc vaporization. Much of this power is recovered at the edges of the pool as the vapor condenses. Because of this evaporation-condensation process it is very difficult to determine the absolute vaporization rate with any accuracy.

Schauer *et al.* used an infrared pyrometer to measure the weld pool surface temperature of electron beam welds in steel and aluminum.[11] If one assumes that the power lost from the electron beam weld pool is 6000 watts · cm^{-2}, the measured temperatures are in reasonable agreement with the values predicted by the model presented here as seen in Table IV. Indeed, these results are perhaps the most conclusive in showing that evaporative power losses set an upper limit on the surface temperature of a weld pool. In general, these power losses probably lie between 1 and 10 pct of the total power, but the value varies somewhat with alloy content and with input power density. These losses provide a prediction of maximum arc weld pool surface temperatures between the melting point and 1600 °C for aluminum alloys and between 2000 °C and 2500 °C for steels. The high energy density processes such as laser and electron beam can produce even higher surface temperatures with greater rates of alloy vaporization than arc welds.

VI. CONCLUSIONS

A thermodynamic model of vaporization from weld pools has been presented which can predict the dominant metal vapors that form during welding in the absence of strong compound forming elements such as oxygen or nitrogen. The evaporative power loss in arc welding lies between 1 and 10 pct of the incident power, although more precise measurement is difficult due to condensation of metal vapors in cooler regions of the weld pool. These vaporization rates place upper limits on the surface temperature of the weld pool. These limits are in good agreement with measurements on different alloys when using electron beam welding, but the results for arc welding are somewhat lower than the temperatures often assumed for arc weld pools. It is concluded that the metal vaporization from the weld pool places a limit on the maximum temperature of the pool which is significantly less than the boiling temperature of the metal. The presence of volatile alloying elements may further reduce this maximum temperature limit.

Table IV indicates that apparent evaporation rates (initial and mean) confirm Zn domination of the group I alloys, Mg domination in group II, and co-domination of Zn and Mg in group III alloys.

The largest absolute evaporation seen occurs in the Zn dominated group I followed by Mg dominated group II. The apparent percentages of the total energy are very small indicating that the vapors are subjected to multiple recycling during extended time arc welding.

Table IV. Comparison of Predicted Welding Temperatures and Temperatures Measured by Schauer *et al.*[11]

Al-Alloy, Steel or Metal	Maximum Predicted Temperatures (CSM) if 10 Pct or 100 Pct Energy Went into Evaporation	Dominating Vapor Species at CSM if 10 Pct Went into Evaporation	Dominating Vapor Species at CSM if 100 Pct Went into Evaporation	Schauer's[11] Electron Beam Temperatures t °C
Aluminum	1775	Al		
	2091		Al	
1100	1614	Zn		1900 ± 100
	2091		Al	(1990 to 2055)*
2024	1290	Mg		1700 ± 100
	1751		Mg	
5083	1126	Mg		1250 ± 100
	1491		Mg	
5456	1104	Mg		
	1451		Mg	
6061	1358	Mg		1800 ± 100
	1882		Mg	(1800 to 1890)*
7075	909	Zn		1080 ± 100
	1242		Zn	(1380 to 1485)*
Steels with 0.5 pct Mn	2190	Mn		2290 ± 60; HY-130 st
	2520		Fe	
Steels with 2.0 pct Mn	2010	Mn		2100 ± 50; 304 st
	2520		Fe	
20-6-9 steel		Mn		1820 ± 40
			Mn	
Tantalum		Ta		4400 ± 150
			Ta	

*Data from Schauer's figures, not matching tabulated temperatures

ACKNOWLEDGMENTS

The authors wish to express their appreciation to the Office of Naval Research for sponsoring this research under contract N00014-C-80-0384, and to Dr. Charly Allemand for assistance with setting up the spectrographic equipment.

REFERENCES

1. D. W. Moon and E. A. Metzbower: *Welding Journal,* 1983, vol. 62, pp. 53s-58s.
2. S. S. Glickstein: *Welding Journal,* 1976, vol. 55, pp. 222s-29s.
3. R. F. Heile and D. C. Hill: *Welding Journal,* 1975, vol. 54, pp. 201s-10s.
4. J. D. Cobine and E. E. Burger: *J. Appl. Phys.,* 1955, vol. 26, pp. 895-900.
5. A. Block-Bolten and T. W. Eagar: *Trends in Welding Research in the United States,* S. A. David, ed., ASM, Metals Park, OH, 1982, pp. 53-73.
6. S. Dushman and J. M. Laferty, eds., 2nd Edition, *Scientific Foundations of Vacuum Technique,* John Wiley, New York, NY, 1962, pp. 691-737 and pp. 15-21.
7. O. H. Nestor: *J. Appl. Phys.,* 1962, vol. 33, pp. 1638-48.
8. N. Christensen, V. Davies, and K. Gjermundsen: *British Welding J.,* 1965, vol. 12, pp. 54-75.
9. M. B. C. Quigley, P. H. Richards, D. T. Swift-Hook, and A. E. F. Gick: *J. Phys., D-Appl. Phys.,* 1973, vol. 6, pp. 2250-58.
10. G. Dunn: M.I.T., Cambridge, MA, unpublished research, 1982.
11. D. A. Shauer, W. H. Giedt, and S. M. Shintaku: *Welding Journal,* 1978, vol. 57, pp. 127s-33s.
12. R. Hultgren, P. D. Desai, D. T. Hawkins, M. Gleiser, and K. K. Kelley: *Selected Properties of Binary Alloys,* ASM, Metals Park, OH, 1973.